Lesion Quantification Using the Local Impulse Response from Embedded Point Source

Yusheng Li, Margaret E. Daube-Witherspoon, Samuel Matej, and Scott D. Metzler

***Abstract*—The measurements of lesion standardized uptake value (SUV) in clinical PET studies are affected in a complicated way on many aspects of the data, including—but not limited to—count level, lesion size, lesion shape, lesion location, background level and structure, and patient size. In addition, the SUVs are also affected by the reconstruction algorithms and their parameters, e.g., number of iterations, parameters of point spread function (PSF) model, post-filtering and regularization parameters for penalized-likelihood reconstructions. Optimized reconstruction algorithms and their parameters can provide substantial improvements in quantification in PET imaging. We would like to study the response of a particular lesion at a particular location, which will be used as a criterion for optimizing the reconstruction parameters. In this study, we use an embedded point source to determine the local impulse response (LIR) at the location of the lesion, and thus characterize the local properties and responses of an imaging system. The determined LIR can then be used by an automatic expert system to determine the optimal parameters for better quantifying a particular lesion in a particular patient. The list-mode point source data can be experimentally acquired from a physical point source using the same PET scanner as was used for the patient data. Data from a point source can then be embedded by merging point source list-mode data into the patient data. To reduce the variability, we fit the estimated LIR using a 3D Gaussian model. The fitted LIR can be convolved with the estimated lesion shape to calculate the lesion bias for a particular lesion in a region of interest (ROI). As an initial study, we convolve known lesions of different sizes with the fitted LIR, and the recovery coefficients (RCs) are computed and compared with the RCs obtained using standard method.**

***Index Terms*—Local impulse response (LIR), embedded point source, expert system, blob, image reconstruction, positron emission tomography (PET).**

I. Introduction

PET imaging combined with CT or MR has been increasingly used to assist cancer diagnosis, stage patient diseases, and drive patient therapy. PET is also an important tool for radio-labelled molecular imaging. Image reconstruction methods have a key role in converting the measured data into meaningful and diagnostically useful images. Many iterative reconstruction algorithms have been developed, but the algorithm that gives the most reliable quantification, e.g., standardized uptake value (SUV), depends in a complicated way on many aspects of the data, including—but not limited to—count level, lesion size, lesion shape, lesion location, background level and structure (e.g., a lesion near the bladder versus the liver), and patient size. In addition, measurements of the SUV in clinical PET studies are also impacted by the choice of reconstruction algorithms and their parameters, e.g., number of iterations, parameters of point spread function (PSF) model, post-filtering and regularization parameters for penalized-likelihood reconstructions. Incorporating resolution modeling in iterative reconstruction improves the accuracy of the estimated SUV; however, it can also increase the variability of the SUV estimations. Optimized reconstruction algorithms and their parameters can provide substantial improvements in reconstruction quantification in PET imaging. The optimizations of these parameters can be complicated and tedious, and we propose an automatic expert system to determine the optimized parameters for quantifying a particular lesion in a particular patient by fully understanding the reconstruction properties and responses.

Manuscript received January 19, 2016.

The authors are with the Department of Radiology, University of Pennsylvania, 3620 Hamilton Walk, Philadelphia, Pennsylvania 19104 USA (e-mail: yushli@upenn.edu).

This work was supported in part by the National Institute of Biomedical Imaging and Bioengineering (NIBIB) of the National Institutes of Health (NIH) under award number R21EB021559.

II. Materials and Methods

A. Iterative Local Impulse Response

For an idealized tomography system, one can use the point spread function (PSF) to fully characterize the system [1]. However, for real imaging systems, the system response is spatially variant, object-dependent, and nonlinear, which makes the system property study cumbersome. We would like to study a particular lesion response at a particular location. The local impulse response (LIR) is a useful tool for investigating the local response properties of an imaging system and the reconstruction algorithm used to reconstruct the images [2]–[5]. The local impulse response is defined in terms of the mean reconstruction $\boldsymbol{\mu}^{(k)}(\boldsymbol{f})$ of object $\boldsymbol{f}$ and is the limiting difference between the reconstructions of an object and its perturbation with a point source, $\boldsymbol{\mu}^{(k)}(\boldsymbol{f}+\delta\boldsymbol{e}_j)$. The local impulse response (LIR) of j-th pixel at iteration k is defined as [3]

$$\boldsymbol{l}_j^{(k)}(\boldsymbol{f}) = \lim_{\delta\to 0}\frac{\boldsymbol{\mu}^{(k)}(\boldsymbol{f}+\delta\boldsymbol{e}_j)-\boldsymbol{\mu}^{(k)}(\boldsymbol{f})}{\delta} = \frac{\partial}{\partial f_j}\boldsymbol{\mu}^{(k)}(\boldsymbol{f}). \quad (1)$$

In the context of emission tomography, it was observed that LIR is approximately locally invariant [5]–[8]. For a small lesion, one LIR located near the center of the lesion can be used; one can always use multiple LIRs for a relatively large lesion for better quantification.

B. Embedded Point Source in List-Mode Data

To estimate LIR, an addition reconstruction with an inserted point source is required. It is infeasible to insert a radioactive

source into patients. Here we use data from a point source, which are synthetically embedded into the patient's list-mode data. Synthetically embedding technique provides a method for adding the data with a lesion of known size, shape, location, and activity concentration into an existing patient data set [9]–[12]. This has the strong advantage of phantom studies: known truth and all physical effects inherently included because of its experimental acquisition; it also has the advantage of clinical relevance since each patient's data will be used, inherently mimicking the circumstances for a particular lesion.

Instead of embedding an artificial lesion of similar size, we synthetically embed data from a point source measured in air at a location near the lesion. This will give us two data sets: with and without the embedded point source. We then reconstruct both sets and take the difference to estimate the local impulse response (LIR) in image space. The list-mode data of a point source can be experimentally acquired from a physical point source using the same PET scanner as acquiring the patient data. List-mode events from the point source are merged into the patient's list-mode data. To compensate for attenuation by the patient, the point source list-mode data are reduced prior to merging by randomly rejecting events based on the probability of attenuation along each event's line of response.

C. 3D Gaussian Fitting

Due to the counts limited nature of PET (or SPECT) images, the estimated local impulse response (LIR) can be noisy for the low counts cases. We use a 3D Gaussian model to fit the estimated LIR along the radial, tangential and axial directions. Specifically, the 3D Gaussian model is

$$\begin{aligned}&\mathrm{PSF}(\boldsymbol{x};\boldsymbol{\mu},\boldsymbol{\Sigma})\\ &= C\frac{1}{(2\pi)^{3/2}|\boldsymbol{\Sigma}|^{1/2}}\exp\left[-\frac{1}{2}(\boldsymbol{x}'-\boldsymbol{\mu})^{\mathsf{T}}\boldsymbol{\Sigma}^{-1}(\boldsymbol{x}'-\boldsymbol{\mu})\right],\\ &\qquad \boldsymbol{\mu}=(\mu_r,\mu_t,\mu_\xi)^{\mathsf{T}},\ \boldsymbol{\Sigma}=\mathrm{diag}\big(\sigma_r^2,\sigma_t^2,\sigma_\xi^2\big). \quad (2)\end{aligned}$$

Here, C is a constant, $\boldsymbol{x}'=(r,t,\xi)^{\mathsf{T}}$ is the LIR coordinates respectively along radial, tangential and axial directions, which can be obtained by rotating the image space coordinates $\boldsymbol{x}$. For an LIR with a complex shape, e.g., the LIR of an limited-angle imaging system, a Gaussian mixture model (e.g., two 3D Gaussians) can be used to fit the LIR [13]. We use a nonlinear least-squares method to fit the seven parameters of a 3D gaussian.

To characterize the spatial resolution of an LIR, we use a 3D full width at half maximum (FWHM) metric. The 3D FWHM is the geometric mean of the FWHMs along radial, tangential and radial directions (the diameter of an equivalent sphere):

$$\mathrm{FWHM}_{3\mathrm{D}}=\sqrt{\log 256}\times(\sigma_r\sigma_t\sigma_\xi)^{1/3}. \quad (3)$$

D. Simulation Setup and Digital Phantom

We used EGS4 to generate list-mode data for a generic whole-body PET scanner with time-of-flight (TOF) information [14], [15]. As shown in Fig. 1, a cylindrical phantom of $35\,\mathrm{cm}$ diameter containing a $10\,\mathrm{cm}$ diameter cold cylinder with lung-like attenuation (linear attenuation coefficient $0.32\,\mathrm{cm}^{-1}$) was used in the simulations. Two spheres with $22\,\mathrm{mm}$ diameters were embedded in the phantom with a 3:1 activity ratio with respect to the warm background, one offset from the center of the lung cylinder and the other in the warm background. Trues-only data with TOF resolution of $300\,\mathrm{ps}$ were simulated; randoms and scatter were not considered in this study. The data were reconstructed using the list-mode TOF ordered subsets expectation maximization (OSEM) algorithm with 25 subsets and 10 iterations. Blob-based reconstructions with Kaiser-Bessel basis functions were used. The blob images were reconstructed on a body-centered cubic (BCC) grid with step size of $6\,\mathrm{mm}$; and the the blob images were then converted to voxel images with voxel size of $2\,\mathrm{mm}$ with no post-filtering. This algorithm and parameters closely replicates what is used clinically for whole-body PET studies at our institution. We used a shifted body centered cubic (BCC) grid that allows the point source be sampled by one sampling point of the BCC grid (i.e., centered on a single blob).

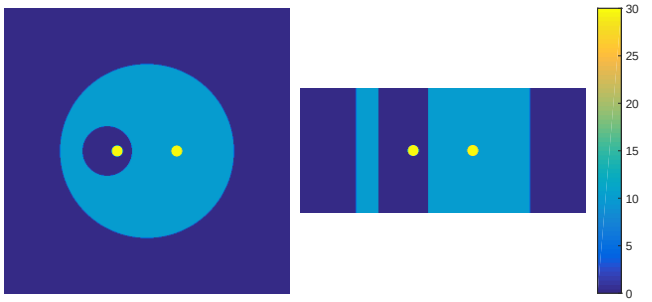

Fig. 1. The digital phantom of $35\,\mathrm{cm}$ diameter is used in the simulation. This phantom contains two $22\,\mathrm{mm}$ spheres with 3:1 activity ratio with respect to the average background uptake.

We simulated 100 independent realizations of the phantoms, each with 1×10^7 true events. We performed reconstructions with 10 different independent realizations as the starting dataset in order to determine the variability.

III. Results

A. The Estimated Local Impulse Response

Typical reconstructed images with and without the embedded point source are shown in Fig. 2. The embedded source is located in the center of the sphere at $6\,\mathrm{cm}$ along x axis in the warm background. An embedded point source with total counts of 1k was embedded in the list-mode data of the phantom for this noisy reconstruction.

By taking the difference of the two reconstructed images with and with the embedded point source, we obtain the local impulse response (LIR) as shown in Fig. 3(a). We then fitted the estimated LIR with the 3D Gaussian model (2). The profiles along radial, tangential, and axial directions, as well as the 3D Gaussian fitted curves, are shown in Fig. 3(b).

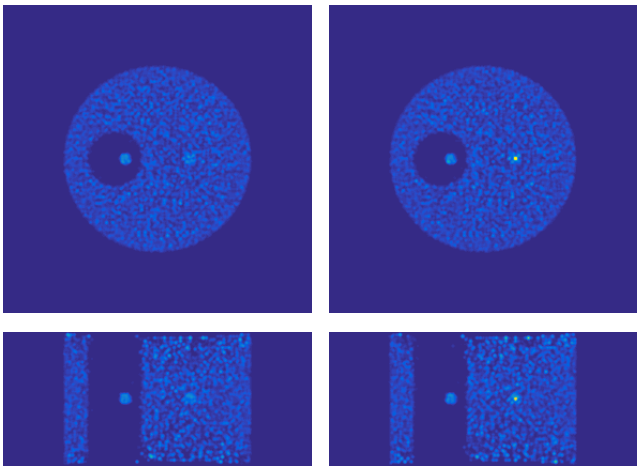

(a) Without point source (b) With point source

Fig. 2. Comparison of noisy reconstructions with and without embedded point source. The phantom is 35 cm in diameter, and the point source is shift 6 cm along x axis.

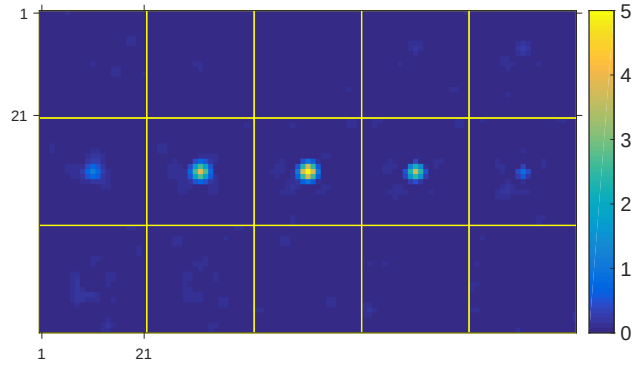

(a) Estimated LIR

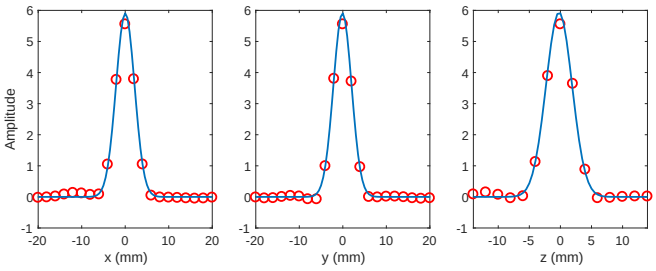

(b) Profiles and 3D Gaussian fitting

Fig. 3. The 3D LIR is determined by taking the difference of the reconstructions with and with the embedded point source. The detected count of the embedded point source was 2k in this estimated LIR. The maker (○) indicates the measured LIR and the curve is the 3D Gaussian fitting.

B. Impact of Counts of the Embedded Point Source

The amount of activity from the embedded point source should be as small as possible since iterative reconstructions are object-dependent and nonlinear. However, using a small number of detected point source events can produce a very noisy LIR. We investigated the impact of the detected counts of the embedded point source on the estimation of LIR. We merged list-mode data with different number of counts for the

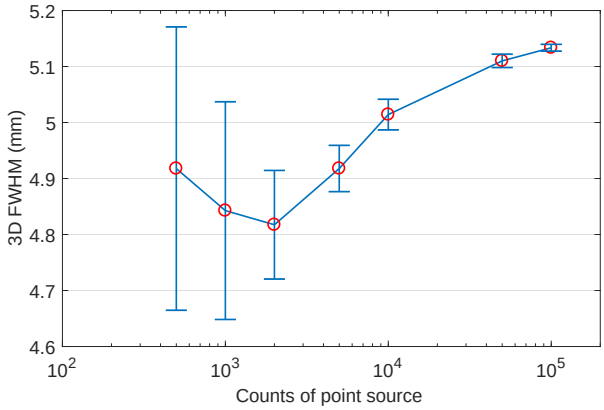

(a) Point source in lung

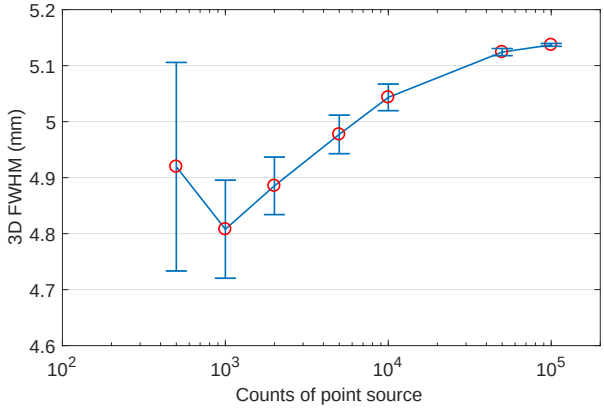

(b) Point source in warm background

Fig. 4. Calculated 3D FWHM versus number of detected counts from the embedded point source. The error bas shows the standard deviation of 10 estimated LIRs.

point sources at two locations: lung and warm background; the numbers of detected events from the point source after phantom attenuation are: 500, 1k, 2k, 5k, 10k, 50k, 100k. There were 10 noise realizations for each count level of the point source for each location. We fitted the 10 estimated LIRs with a Gaussian model and calculated the 3D FWHM. Fig. 4 shows the calculated 3D FWHM versus the numbers of detected counts in the embedded point source. The error bar shows the standard deviation of the 10 estimated LIRs. From the figure, we see high counts of the point source can affect the reconstruction and 3D FWHM estimation; low counts can produce LIR with large variance. The 1k or 2k counts can be good choices for the LIR estimation. The number of count is 1k in the image shown in Fig. 2(b).

C. The Estimated Recovery Coefficients

The LIR can be useful to characterize the local properties and responses of a reconstruction algorithm or an imaging system. To demonstrate the usefulness, we convolved the fitted LIR with ideal lesion spheres and then the recovery coefficient (RC) were calculated inside the lesion spheres. Six sphere diameters (10, 13, 17, 22, 28 and 37 mm) were considered, which span the range of lesion sizes typically encountered in clinical PET imaging.

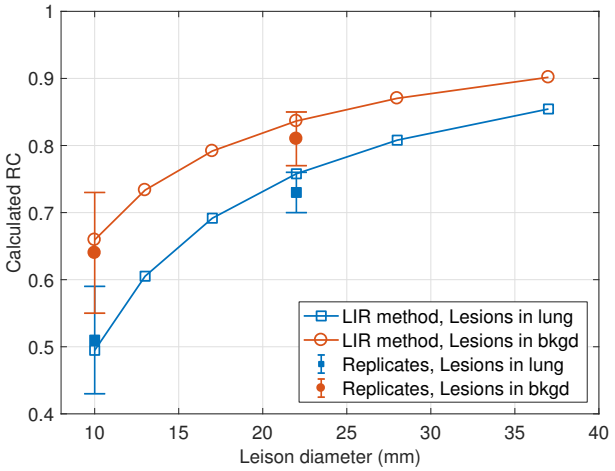

Fig. 5. Calculated the recovery coefficients (RCs) for different sizes of lesions in lung and in warm background.

Fig. 5 shows the calculated RCs for different sizes of lesions in lung and in warm background using the 3D FWHM estimated from 2k point source events. The solid symbols show results measured in the same phantom for 10 and 22 mm diameter spheres; the error bars are the standard deviation over 100 independent noisy realizations. There is some difference between the estimated RCs using the LIR method and the RCs computed from noise realizations, but the difference is within the uncertainty [15].

IV. Discussion and Conclusion

The local impulse response (LIR) can be very useful to characterize the local properties and responses of an imaging system for quantifying a particular lesion. The advantages of the LIR methods is that it allows much more flexibility compared to the method of inserting pre-acquired spheres because the size and shape of the lesion are unlimited by this method, whereas only a limited number of spherical lesions can be acquired using the lesion inserting technique. Using experimentally acquired point sources inherently takes all physical effects into account. We have also investigated using the bootstrapping method to estimate the variability of lesion uptake for both the mean and maximum uptake [15]. Further work will include the studies of using other systematic and statistical methods to fully understand the intrinsic responses and statistical properties of reconstruction algorithms.

We presented in this work that an local impulse response can be estimated using an embedded point source. The embedded point source was synthetically embedded into phantom list-mode data. The local properties and responses of a reconstruction algorithm or an imaging system can be characterized by the LIR. We have demonstrated that the recovery coefficient of lesions with different sizes can be computed from the fitted LIR, which can be useful for quantifying the lesion and bias correction of the uptake values in patient studies.

Acknowledgment

We would like to thank Mr. Matthew E. Werner for useful discussions regarding the selection of blob and grid parameters for the blob-based image reconstructions.

References

[1] G. T. Gullberg and T. F. Budinger, "The use of filtering methods to compensate for constant attenuation in single-photon emission computed-tomography," *IEEE Trans. Biomed. Eng.*, vol. 28, no. 2, pp. 142–157, 1981.

[2] J. A. Stamos, W. L. Rogers, N. H. Clinthorne, and K. F. Koral, "Object-dependent performance comparison of two iterative reconstruction algorithms," *IEEE Trans. Nucl. Sci.*, vol. 35, no. 1, pp. 611–614, 1988.

[3] J. A. Fessler and W. L. Rogers, "Spatial resolution properties of penalized-likelihood image reconstruction: Space-invariant tomographs," *IEEE Trans. Image Process.*, vol. 5, no. 9, pp. 1346–1358, Sep. 1996.

[4] J. W. Stayman and J. A. Fessler, "Compensation for nonuniform resolution using penalized-likelihood reconstruction in space-variant imaging systems," *IEEE Trans. Med. Imag.*, vol. 23, no. 3, pp. 269–284, Mar. 2004.

[5] ——, "Efficient calculation of resolution and covariance for penalized-likelihood reconstruction in fully 3-D SPECT," *IEEE Trans. Med. Imag.*, vol. 23, no. 12, pp. 1543–1556, Dec. 2004.

[6] J. Fessler and S. Booth, "Conjugate-gradient preconditioning methods for shift-variant pet image reconstruction," *IEEE Trans. Image Process.*, vol. 8, no. 5, pp. 688–699, May 1999.

[7] J. Y. Qi and R. M. Leahy, "Resolution and noise properties of MAP reconstruction for fully 3-D PET," *IEEE Trans. Med. Imag.*, vol. 19, no. 5, pp. 493–506, May 2000.

[8] Y. Li, "Noise propagation for iterative penalized-likelihood image reconstruction based on Fisher information," *Phys. Med. Biol.*, vol. 56, no. 4, pp. 1083–1103, Feb. 2011.

[9] G. El Fakhri, S. Surti, C. M. Trott, J. Scheuermann, and J. S. Karp, "Improvement in lesion detection with whole-body oncologic time-of-flight PET," *J. Nucl. Med.*, vol. 52, no. 3, pp. 347–353, Mar. 2011.

[10] S. Surti, J. Scheuermann, G. El Fakhri, M. E. Daube-Witherspoon, R. Lim, N. Abi-Hatem, E. Moussallem, F. Benard, D. Mankoff, and J. S. Karp, "Impact of time-of-flight PET on whole-body oncologic studies: a human observer lesion detection and localization study," *J. Nucl. Med.*, vol. 52, no. 5, pp. 712–719, May 2011.

[11] M. E. Daube-Witherspoon, S. Surti, A. E. Perkins, and J. S. Karp, "Determination of accuracy and precision of lesion uptake measurements in human subjects with time-of-flight PET," *J. Nucl. Med.*, vol. 55, no. 4, pp. 602–607, Apr. 2014.

[12] Y. Li, M. E. Daube-Witherspoon, J. S. Karp, S. Surti, S. Matej, and S. D. Metzler, "Modulating time-activity curves for different compartments in list-mode data," in *13th Int. Conf. on Fully 3D image Reconstruction in Radiology and Nuclear Medicine*, Newport, RI, Jun. 2015, pp. 550–553.

[13] S. Matej, Y. Li, J. Panetta, J. S. Karp, and S. Surti, "Image-based modeling of PSF deformation with application to limited angle PET data," *IEEE Trans. Nucl. Sci.*, vol. 63, no. 5, pp. 2599–2606, Oct. 2016.

[14] L. E. Adam, J. S. Karp, and G. Brix, "Investigation of scattered radiation in 3D whole-body positron emission tomography using Monte Carlo simulations," *Phys. Med. Biol.*, vol. 44, no. 12, pp. 2879–2895, Dec. 1999.

[15] M. E. Daube-Witherspoon, J. S. Karp, S. Matej, Y. Li, and S. D. Metzler, "Estimating the precision of lesion uptake measurements," in *submitted to 14th Int. Conf. on Fully 3D image Reconstruction in Radiology and Nuclear Medicine*, Xi'an, Shaanxi, China, Jun. 2017.